Binding Site Analysis of Cellulose Binding Domain CBD_{N1} from Endoglucanse C of *Cellulomonas fimi* by Site-Directed Mutagenesis†

Jeff Kormos,‡ Philip E. Johnson,§ Emmanual Brun,§ Peter Tomme,‡ Lawrence P. McIntosh,§,|| Charles A. Haynes,⊥,▽ and Douglas G. Kilburn*,‡,⊥

Departments of Microbiology and Immunology, Chemistry, Biochemistry and Molecular Biology, and Chemical Engineering and Biotechnology Laboratory, University of British Columbia, Vancouver, British Columbia, Canada, V6T 1Z3

Received March 16, 2000

ABSTRACT: Endoglucanase C (CenC), a β1,4 glucanase from the soil bacterium *Cellulomonas fimi*, binds to amorphous cellulose via two homologous cellulose binding domains, termed CBD_{N1} and CBD_{N2}. In this work, the contributions of 10 amino acids within the binding cleft of CBD_{N1} were evaluated by single site-directed mutations to alanine residues. Each isolated domain containing a single mutation was analyzed for binding to an insoluble amorphous preparation of cellulose, phosphoric acid swollen Avicel (PASA), and to a soluble glucopyranoside polymer, barley β-glucan. The effect of any given mutation on CBD binding was similar for both substrates, suggesting that the mechanism of binding to soluble and insoluble substrates is the same. Tyrosines 19 and 85 were essential for tight binding by CBD_{N1} as their replacement by alanine results in affinity decrements of approximately 100-fold on PASA, barley β-glucan, and soluble cellooligosaccharides. The tertiary structures of unbound Y19A and Y85A were assessed by heteronuclear single quantum coherence (HSQC) spectroscopy. These studies indicated that the structures of both mutants were perturbed but that all perturbations are very near to the site of mutation.

Cellulose is degraded to cellobiose units by the synergistic action of several enzymes, collectively termed as cellulases. Cellulases have evolved as modular enzymes; most contain a catalytic domain (CD)[1] responsible for the hydrolysis of cellulose and usually one or more cellulose binding domains (CBD) that mediate binding of the enzyme to cellulose but are devoid of hydrolytic activity. Both domain types are the focus of independent classification systems that organize CD (*1*−*4*) and CBD sequences (*5*−*7*) into separate families by sequence homology.

The roles of CBDs in cellulose degradation are still being elucidated. One obvious function of these binding domains is to keep cellulases in close contact with their substrate. Removing a CBD severely impairs the activity of a cellulase on insoluble substrates but has little effect on the degradation of soluble substrates (*8*−*13*). This suggests that the presence of a CBD is important for the efficient degradation of natural cellulose. CBDs may also be involved in the disruption of cellulose fibers by nonhydrolytic means (*14*, *15*).

The structures of seven CBDs are known. These include the crystal structures of CBD_{CipB} from *Clostridium thermocellum* (*16*) and CBD_{E4} from *Thermomonospora fusca* (*17*), and the NMR structures of CBD_{CBHI} from *Trichoderma reseei* (*18*), CBD_{Cex} (*19*), CBD_{N1} (*20*), and CBD_{N2} (*59*) from *Cellulomonas fimi*, and CBD_{EGZ} from *Erwinia chrysanthemi* (*21*). The CBDs from CBHI, Cex, E4, CipB, and EGZ, representing CBD families I, II, III, and V, respectively, all show a planar surface that is responsible for binding to crystalline cellulose. Surface-exposed aromatic residues, flanked by additional polar amino acid side chains, are present on each of the proposed binding surfaces. Site-directed mutagenesis has been used to confirm that tyrosines are critical for the binding of family I CBD_{CBHI} to crystalline cellulose (*22*, *23*), whereas tryptophans direct the binding of family II CBDs (*24*−*27*).

Endoglucanase C from *Cellulomonas fimi* contains two family IV CBDs, CBD_{N1} and CBD_{N2}, that are present in tandem at its N-terminus. The structures of CBD_{N1} and CBD_{N2} differ from most other CBDs as they contain a binding cleft rather than a planar binding face (*28*). CBD_{N1}

† This work is supported in part by a grant from the Natural Science and Engineering Research Council of Canada and the Protein Engineering Network of Centers of Excellence.

* To whom correspondence should be addressed at the Department of Microbiology and Immunology, #300-6174 University Blvd., Vancouver, British Columbia, Canada V6T 1Z3. Phone (604) 822-4182; fax: (604) 822-6041; e-mail kilburn@unixg.ubc.ca.

‡ Department of Microbiology and Immunology.

§ Department of Chemistry.

|| Department of Biochemistry and Molecular Biology.

⊥ Biotechnology Laboratory.

▽ Department of Chemical Engineering.

[1] Abbreviations: CD, catalytic domain; CBD, cellulose binding domain; CBD_{N1}, N-terminal cellulose binding domain from *Cellulomonas fimi* endoglucanase C; PASA, phosphoric acid swollen Avicel; BMCC, bacterial microcrystalline cellulose; HEC, hydroxyethylcellulose; HPMC, hydroxypropylmethylcellulose; CMC, carboxymethylcellulose; DP, degree of polymerization; NMR, nuclear magnetic resonance; HSQC, heteronuclear single quantum coherence; IPTG, isopropyl β-D-thiogalactoside; PCR, polymerase chain reaction; Kan^R, kanamycin resistance; LacI, *lac* repressor protein; P_{tac}, hybrid promoter composed of regions from the tryptophan and lactose operons; L_x, leader sequence from the *C. fimi* cellobiohydrolase, Cex; A_{280}, sample absorbance at 280 nm; *F*, concentration of free protein; *B*, concentration of bound protein; K_a, association constant; K_d, dissociation constant; N_o, concentration of binding sites on the substrate; rm, relative migration distance; BPB, bromophenol blue; BSA, bovine serum albumin; SDS, sodium dodecyl sulfate; DTT, dithiothreitol; DSC, differential scanning calorimetry; ITC, isothermal titration calorimetry.

10.1021/bi000607s CCC: $19.00
Published on Web 07/06/2000

binds to phosphoric acid swollen Avicel (PASA) but does not bind appreciably to either bacterial microcrystalline cellulose (BMCC) or Avicel (*5*, *29*). CBD_{N1} also binds to a wide range of soluble cellulosics, including hydroxyethylcellulose (HEC), hydroxypropylmethylcellulose (HPMC), carboxymethylcellulose (CMC), oat β-glucan, barley β-glucan, and cellooligosaccharides with DPs of 3 or greater (*28*, *29*). Binding affinities rise markedly as the cellooligosaccharide length is increased from cellotriose to cellopentaose. No further increase in binding affinity is observed with longer chain cellooligosaccharides, indicating that five saccharide units are sufficient to span the binding cleft of CBD_{N1} (*28*, *29*). The CBD also has little preference for sugar orientation; cellooligosaccharide substrates may bind in either direction lengthwise across the binding cleft (*30*).

Thermodynamic analysis revealed that the binding of CBD_{N1} to PASA, cellooligosaccharides, and soluble cellulosics is enthalpically driven with an unfavorable entropic contribution (*29*, *31*), suggesting that hydrogen-bonding and van der Waals interactions mediate the binding of this CBD to single chains of cellulose. In contrast, the binding of CBD_{Cex} to BMCC is entropically driven, presumably due to dehydration at the binding interface (*32*).

Despite substantial structural and functional characterization, many questions remain regarding the precise mechanism of CBD_{N1} binding. On the basis of amide chemical shift perturbations and unassigned intermolecular nuclear Overhauser enhancement (NOE) interactions, a preliminary model of CBD_{N1} binding to cellooligosaccharides was developed (*28*, *29*). In this model, the glucopyranosyl rings of the cellulose chain stack on a central strip of hydrophobic residues within the binding cleft of CBD_{N1}, while flanking polar groups form hydrogen bonds to equatorial hydroxyls. The contribution of one or more tyrosine residues to this binding model was also indicated qualitatively by UV absorption spectroscopy (*29*). It is the purpose of this work to test the current binding hypothesis by site-directed mutagenesis of polar and aromatic amino acids within the binding cleft. Ten putative binding-site residues, including Y19 and Y85, were individually mutated to alanine and analyzed for their relative contribution toward the affinity of CBD_{N1} for soluble and insoluble cellulosic ligands (Figure 1). The effect of these mutations on the structure of CBD_{N1} was also examined by one and two-dimensional NMR spectroscopy.

EXPERIMENTAL PROCEDURES

Reagents. Kanamycin, cellopentaose, isopropyl β-D-thiogalactoside (IPTG), and barley β-glucan were all purchased from Sigma. ^{15}N-labeled Celtone and $(^{15}NH_4)_2SO_4$, respectively, were from Martek Biosciences and Cambridge Isotopes. *Vent* polymerase and DNA ligase were obtained from New England Biolabs. Deoxynucleoside triphosphates used in the PCR reactions were products of Gibco−BRL. Avicel PH101 was from FMC International; phosphoric acid swollen Avicel (PASA) was prepared by a protocol from Wood (*33*).

Plasmids and Bacterial Strains. pTug, a vector described previously (*28*, *34*), was used for the cloning and expression of CBD_{N1} variants. *Escherichia coli* strains JM101 (*supE thi-1* Δ(*lac*−*proAB*) [*F′ traD36 proAB lacI*^{q}*Z*Δ*M15*]) (*35*) and DH5α (*F*$^-$; *endA1 hsdR17(rk mk*$^+$*) supE44 thi-1 recA1 gyrA96 relA1* (*argF*−*lacZYA*)*U169* ϕ*lacZ M15*) (*36*) were used as host strains. *E. coli* DH5α was used to prepare DNA for cloning and sequencing; *E. coli* JM101 was used exclusively for protein production. IPTG, at a final concentration of 0.2 mM, was used to induce gene expression.

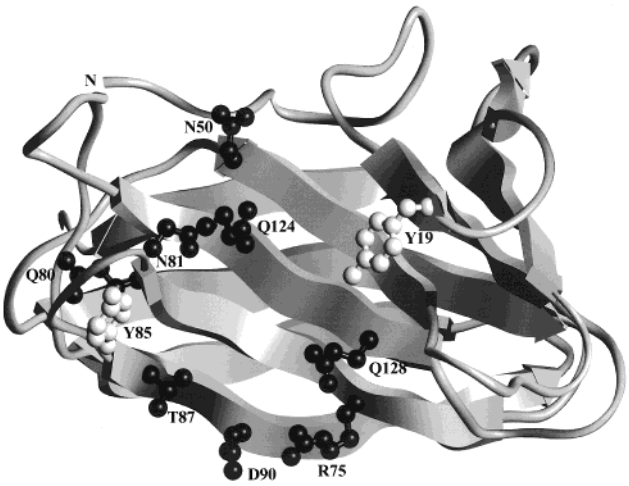

FIGURE 1: Molscript ribbon diagram of the NMR-derived structure of CBD_{N1} (*20*), highlighting the binding site residues investigated in this mutagenic study. This perspective views the open binding cleft from above.

DNA Methods. Various molecular cloning techniques were performed with the appropriate enzymes as directed by suppliers. Each polymerase chain reaction (PCR) mixture (50 μL total volume) contained 10−100 ng of pTugN1 DNA, 10−150 pmol of primers, 10% DMSO, 0.2 mM 2′-deoxynucleotide 5′-triphosphates, and 1 unit of *Vent* polymerase (New England Biolabs) in 10 mM KCl, 10 mM $(NH_4)_2SO_4$, 20 mM Tris-HCl, 2 mM $MgSO_4$, and 0.1% Triton X-100. Twenty-five cycles were performed as follows: denaturation at 95 °C for 30 s, annealing at 55 °C for 30 s, and primer extension at 72 °C for 30 s. PCR products were digested with suitable restriction enzymes and cloned into gel-purified pTug vectors containing a kanamycin resistance cassette. Positive clones were identified by restriction analysis and verified by DNA sequencing.

Protein Expression and Purification. Native CBD_{N1} was purified from culture supernatants by affinity purification on Avicel (*20*, *28*, *29*). This procedure would not be applicable for mutants with low affinity for cellulose. Consequently, a novel expression protocol was developed to maximize the yield of CBD in *E. coli* JM101 periplasms for extraction and subsequent purification by ion-exchange chromatography.

Frozen cell stocks of *E. coli* JM101 transformed with pTugN1 or mutant (*28*) were used to inoculate 2 mL of tryptone/yeast extract (TY) medium supplemented with kanamycin at 100 μg/mL. These cultures were grown overnight at 28 °C until the A_{600nm} was between 5 and 8. Then, 0.8 mL of the culture was used to inoculate 400 mL of TY medium containing 100 μg/mL kanamycin. The cultures were incubated at 28 °C with shaking at 250 rpm and monitored for growth. At mid-log phase (A_{600nm} between 0.1 and 0.5), the cultures were induced with IPTG at 0.2 mM. The cells were then incubated an additional 22 h at 28 °C with shaking at 250 rpm.

Protein was recovered from the periplasm by osmotic shock (*37*) and purified by anion-exchange chromatography. Correct processing of the leader sequence was verified by N-terminal amino acid sequencing of the purified CBD. Osmotic shock fractions were applied to a XK16 (1.6 × 20 cm) column (Pharmacia) packed with 10 mL of macro Q anion-exchange resin (Bio-Rad). Columns were equilibrated in 25 mM phosphate/acetate buffer, pH 5.2; bound protein was eluted with a linear gradient of NaCl (0−1 M, 90 min) in the same buffer at a flow rate of 1.25 mL/min. CBD_{N1} was quantified by A_{280} measurements, using an extinction coefficient of 21 370 cm^{-1} M^{-1} (*31*). Yields for wild-type CBD_{N1} and mutants were consistently between 30 and 40 mg/L of culture except for R75A (3 mg/L) and D90A (60 mg/L). Purified protein preparations were greater than 95% pure, as determined by densitometric measurements on SDS−13% polyacrylamide gels (data not shown).

Determination of Affinity Constants on PASA. Adsorption isotherm assays, as described previously (*29*), were used to generate binding data for CBD_{N1} and mutants on PASA. Each isotherm was constructed from 20 data points, each data point corresponding to the measured concentration of free protein and calculated concentration of bound protein from a binding reaction between CBD and PASA. Binding equilibria were measured in duplicate at 10 different protein concentrations. The equilibrium association constant was determined by nonlinear regression (GraphPad Prism software) of the isotherm data with the following Langmuir-type binding model:

$$[B] = \frac{[N_o]K_a([F] - G)}{1 + K_a([F] - G)} - G \quad (1)$$

where K_a is the association constant (reciprocal molarity), [B] is the concentration of bound protein (micromoles per gram of cellulose), [F] is the concentration of free protein (molarity) and $[N_o]$ is the total concentration of binding sites (moles per gram of cellulose). The variable G is included as a control for optical effects caused by the presence of fine particles of cellulose.

Calculation of Affinity Constants on Barley β-Glucan. Affinity constants for wild-type and mutant CBDs on barley β-glucan were determined by the technique of affinity electrophoresis (*38*−*40*). All electrophoresis experiments were performed with the Modular Mini-Protean II electrophoresis system (Bio-Rad) with 0.75 mm spacers and combs (*29*). Electrophoresis was carried out at 65 V in an ice bath and continued until the bromophenol blue (BPB) dye front was less than 0.5 cm from the bottom of the separating gel. The binding temperature was taken as the temperature of the running buffer within the inner electrophoresis chamber.

Electrophoresis was carried out on each mutant with a minimum of eight polyacrylamide gels containing different concentrations of barley β-glucan. Two of these gels were devoid of barley β-glucan and served as controls. The other gels were set up in duplicate, each with a barley β-glucan concentration between 6 and 662 μM. All solutions of barley β-glucan were prepared from powder immediately before use. Protein samples (10 μL) were composed of 3 μg of purified protein in loading buffer (18% glycerol, 18% bromophenol blue, and 120 mM Tris-HCl, pH 8.8). Acetylated bovine serum albumin (BSA) (3 μg), in loading buffer, was included in one lane of each gel as a control.

Gels were stained [2.5 g/L Coomassie brilliant blue R-250 (Sigma) in 40% methanol and 10% acetic acid] for 20 min and destained (40% methanol and 10% acetic acid) until bands were clearly visible. After drying, the relative migration distance (rm) was calculated as the ratio of the distance migrated by protein to that of the tracking BPB band.

Affinity constants were determined on the basis of a theory of affinity electrophoresis developed previously (*38*−*40*). The theory assumes that an equilibrium is established within the gel, where

$$PL \rightleftharpoons P + L \quad (2)$$

and

$$K_a = [PL]/[P][L] \quad (3)$$

K_a is the equilibrium association constant, and [P], [L], and [PL] are the concentrations of protein, ligand, and the protein−ligand complex, respectively.

Affinity electrophoresis theory also assumes that the protein−polymer complex has a mobility of zero and that the concentration of ligand is large relative to that of protein. If the above conditions apply, the following equation can be derived (*38*, *39*):

$$\frac{1}{rm_i} = \frac{1}{rm_o}(1 + [L]_T K_a) \quad (4)$$

where rm_i and rm_o are the relative migration distances of protein in the presence and absence of polymer, respectively, and $[L]_T$ is the total concentration of ligand. Plots of $1/rm_i$ against $[L]_T$ yield a straight line with an x-intercept equivalent to $-1/K_a$. The binding constants generated have units of $molar^{-1}$ substrate. These units were later converted to $molar^{-1}$ binding site on the basis of the observed stoichiometry of four molecules of CBD_{N1} per barley β-glucan chain at saturation (*29*).

NMR Spectroscopy. One-dimensional ^1H NMR spectra were acquired on samples of wild-type CBD_{N1} and all alanine mutants, as described previously (*20*, *28*).

A more rigorous characterization of wild-type CBD_{N1}, Y19A, and Y85A was performed by $^1H-^{15}N$ HSQC spectroscopy. *E. coli* JM101 cultures expressing Y19A and Y85A, isotopically labeled with ^{15}N, were prepared as described previously (*28*). Periplasmic fractions were combined with the supernatant fractions to increase the yield of isotopically labeled CBD. All protein preparations were fractionated by anion-exchange chromatography (see Experimental Procedures) successively at pH 5.2, pH 7.0, and pH 6.0, with desalting of the column effluent after each pass. Approximately 20 mg of ^{15}N-labeled protein were purified from 1 L of culture. The $^1H-^{15}N$ heteronuclear single quantum coherence (HSQC) spectra for 0.5 mM samples of wild-type CBD_{N1}, Y19A, and Y85A were recorded on a Varian Unity 500 MHz NMR spectrometer at 30 °C. The buffer conditions were 50 mM phosphate buffer, pH 7.0, and 0.05% sodium azide in 90% H_2O/10% D_2O. Analysis was performed with Felix version 2.3 software and involved the comparison of 122 chemical shifts common to CBD_{N1} and the two tyrosine mutants.

Table 1: Measured Affinity Constants (K_a) and Calculated $\Delta\Delta G$ Values for the Binding of CBD_{N1} and Alanine Mutants to PASA and Barley β-Glucan

	PASA[a]		barley β-glucan[b]	
CBD	K_a[c] (M^{-1})	$\Delta\Delta G$[d] (kJ/mol)	K_a[c] (M^{-1})	$\Delta\Delta G$[d] (kJ/mol)
wt CBD_{N1}	$3.8 (\pm 0.3) \times 10^5$ [e]		$3.3 (\pm 0.4) \times 10^4$	
T87A	$1.7 (\pm 0.1) \times 10^5$	1.9	$2.1 (\pm 0.3) \times 10^4$	1.1
Q80A	$1.4 (\pm 0.1) \times 10^5$	2.3	$1.9 (\pm 0.3) \times 10^4$	1.3
D90A	$1.3 (\pm 0.1) \times 10^5$	2.5	$2.0 (\pm 0.2) \times 10^4$	1.2
N81A	$8.1 (\pm 0.7) \times 10^4$	3.6	$7.0 (\pm 0.2) \times 10^3$	3.8
R75A	$6.3 (\pm 0.4) \times 10^4$	4.1	$5.2 (\pm 0.4) \times 10^3$	4.5
Q128A	$5.8 (\pm 0.8) \times 10^4$	4.3	$3.3 (\pm 0.3) \times 10^3$	5.6
Q124A	$5.0 (\pm 0.3) \times 10^4$	4.7	$1.9 (\pm 0.1) \times 10^3$	7.0
N50A	$1.6 (\pm 0.6) \times 10^4$	7.3	$9.2 (\pm 0.4) \times 10^2$	8.7
Y19A	NQ[f]	NQ	$4.6 (\pm 0.1) \times 10^2$	10.4
Y84A	NQ	NQ	$4.2 (\pm 0.2) \times 10^2$	10.7

[a] K_a values were determined from depletion isotherms at 4 °C, pH 7.0. [b] K_a values were determined from affinity electrophoresis where binding temperatures were at least 22 °C, pH 8.8. [c] Values in parentheses indicate deviation from regression analysis with the exception of footnote *e*. [d] $\Delta\Delta G$ values, for each mutant, are calculated from $\Delta\Delta G = -RT \ln (K_{a,mutant}/K_{a,wt})$. [e] K_a value recorded as the average of four depletion isotherms with error as the standard deviation between quadruplicate values. The standard deviation of the affinity constants generated from the four isotherms was 7.07% of the mean affinity constant. K_a values for each mutant were regressed from a single isotherm. [f] NQ indicates that the binding affinity was too low to measure accurately by the depletion isotherm technique.

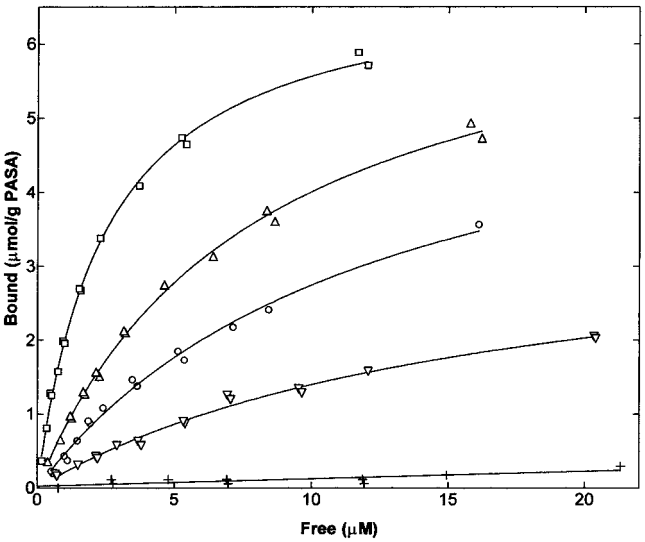

FIGURE 2: Raw adsorption isotherm data and regressed curves for CBD_{N1} (□), and the alanine mutants D90A (△), N81A (○), Q124A (▽), and Y19A (+). Each data point corresponds to an independent binding event involving 1 mg of PASA and 1−25 μM protein. All adsorption experiments were conducted at 4 °C in phosphate buffer, pH 7.0.

The binding constants for the association of cellotetraose and cellopentaose with CBD_{N1} mutants Y19A and Y85A at 30 °C and pH 7 were determined by use of $^1H-^{15}N$ NMR spectroscopy to monitor titrations of the two ^{15}N-labeled proteins with these cellooligosaccharides, as described previously (*28*).

RESULTS

CBD Binding to PASA. All of the mutations tested affected the binding of CBD_{N1} to PASA (Table 1, Figure 2). Alanine replacement at Y19 and Y85 had the largest effect on CBD binding. The affinity of Y19A and Y85A for PASA is so low that affinity constants could not be reliably estimated by nonlinear regression analysis. The weak binding also complicated the extrapolation of an accurate saturation value for the binding of these two mutants to PASA. For all other mutants, the data sets showed convergence on a saturation value, providing good estimates of the binding parameters.

CBD Binding to Barley β-glucan. Affinity electrophoresis was used to generate binding constants on barley β-glucan. In affinity electrophoresis, the interaction between a mobile analyte (i.e., wild-type or mutant CBD_{N1}) and an immobile polymer retards the progress of the analyte through a gel containing polymer (Figure 3). As the concentration of polymer is increased, analyte retardation increases. Figure 4 shows a plot of the retardation data for BSA, wild-type CBD_{N1}, and N81A. Each data point represents the binding data from a single gel at one barley β-glucan concentration. For all mutants, retardation increases linearly with barley β-glucan concentration, in accordance with eq 4. The mobility of BSA remains nearly constant as the concentration of barley β-glucan is increased, indicating that no complexation occurs. Regressed association constants for each mutant are included in Table 1.

Overall, each mutation had a qualitatively similar effect on binding of CBD_{N1} to either PASA or barley β-glucan. Mutants that bound tightly to PASA also bound tightly to barley β-glucan. Similarly, mutants such as Y19A or Y85A that bound weakly to PASA also bound weakly to barley β-glucan (see Table 1). This suggests that the mechanism of CBD_{N1} binding to unbranched soluble and insoluble cellulosic polymers is similar.

CBD Binding to Cellooligosaccharides. Affinity constants for the binding of CBD_{N1} mutants Y19A and Y85A to soluble cellooligosaccharides were also measured by $^1H-^{15}N$ HSQC NMR spectroscopy to monitor the titrations of these proteins with cellotetraose and cellopentaose. As observed with wild-type CBD_{N1}, amides showing the greatest chemical shift perturbations upon addition of sugar were located within the binding groove of the protein (not shown). Although not surprising, this confirms that the amino acid substitutions do not alter the location of the binding site in the mutated CBDs. Fitting of the titration data to eq 1 (Figure 5) yields the association constants reported in Table 2. As also seen with PASA and barley β-glucan, the mutation of either Y19 or Y85 to alanine results in a substantial decrease in binding affinity, indicating that both tyrosines are required for binding to cellopentaose and cellotetraose.

Table 2: Association Constants of CBD_{N1}, Y19A, and Y85A Generated by $^1H-^{15}N$ HSQC NMR Titration Experiments

CBD	cellotetraose	cellopentaose
wt CBD_{N1}	$4.2 (\pm 0.7) \times 10^3$	$3.4 (\pm 0.8) \times 10^4$
Y19A	$8.4 (\pm 1.2) \times 10^1$	$2.7 (\pm 0.3) \times 10^2$
Y85A	$5.9 (\pm 0.8) \times 10^1$	$1.9 (\pm 0.2) \times 10^2$

From Table 2, it is clear that the presence of the fifth D-glucose residue in cellopentaose leads to an order of magnitude increase in binding affinity to wild-type CBD_{N1} (*28*, *29*). Y19A and Y85A are also sensitive to chain length, albeit less sensitive than wild-type CBD_{N1}. This sensitivity of K_a to chain length, regardless of the residue type at positions 19 and 85, indicates that other residues must also interact with the terminal D-glucose residues in cellopentaose.

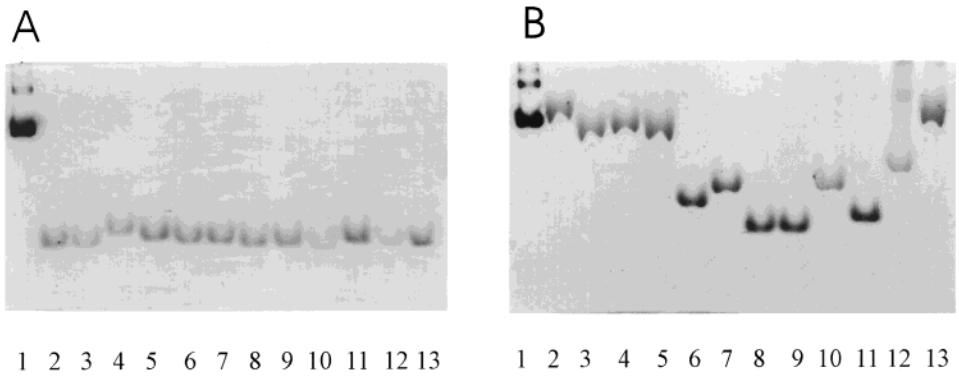

FIGURE 3: Affinity electrophoresis of CBD_{N1} in the presence (B) and absence (A) of barley β-glucan. In each gel, the samples include BSA (lane 1), wt CBD_{N1} (lane 2), T87A (lane 3), D90A (lane 4), Q80A (lane 5), Q124A (lane 6), Q128A (lane 7), Y85A (lane 8), Y19A (lane 9), R75A (lane 10), N50A (lane 11), N81A (lane 12), and wild-type CBD_{N1} (lane 13). Electrophoresis was carried out at 65 V in native gels that contained 13% acrylamide/bisacrylamide in Tris-HCl, pH 8.8, and halted when the bromophenol blue dye front was less than 0.5 cm from the bottom of the separating gel.

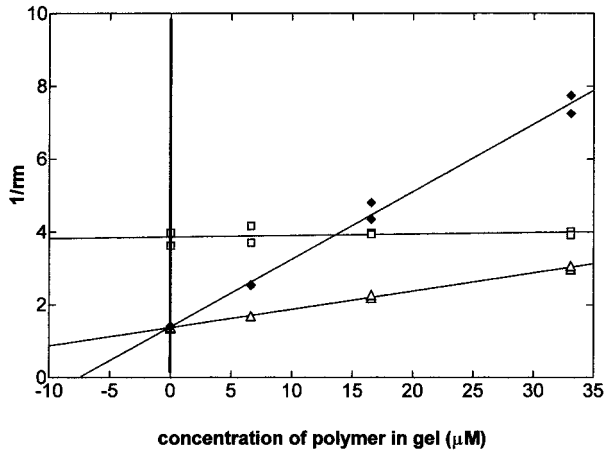

FIGURE 4: Analysis of the affinity electrophoresis data for BSA, CBD_{N1}, and mutants. The relative migration distance (rm) of each protein was measured in native gels (see Experimental Procedures) containing barley β-glucan in 13% acrylamide in Tris-HCl, pH 8.8. The mobility data was converted to a measure of polymer-induced retardation (1/rm) and plotted against barley β-glucan concentration. Curves were generated by linear regression analysis of the raw data, and dissociation constants were determined from the *x*-intercept of the linear regression lines. The analysis was performed for all mutants, though only BSA (□), wtCBD_{N1} (◆), and N81A (△) are included in this figure.

Structural Studies on CBD_{N1} Mutants. NMR spectroscopy was used to assess the structural integrity of CBD_{N1} mutants. The 1D ^1H NMR spectra of each mutant closely resemble that of the wild-type protein and all differ markedly from that of the reduced, unfolded CBD (*41*). Therefore, each CBD_{N1} mutant adopts a well-folded structure under the experimental conditions used in this study. Furthermore, every mutant showed extreme upfield- or downfield-shifted resonances diagnostic of the wild-type protein in its native conformation (*20*). Thus, the amino acid substitutions do not markedly alter the structure of CBD_{N1}. This is consistent with the fact that the mutations involved substitutions of solvent exposed polar or aromatic residues with a single methyl side chain and that each CBD was capable of binding to cellulosic ligands.

To obtain a higher resolution comparison, $^1H-^{15}N$ HSQC spectra were acquired for ^{15}N-labeled wild-type CBD_{N1}, Y85A, and Y19A (Figure 6). Note that amide chemical shifts are exquisitely sensitive to structural perturbations, thus allowing a qualitative yet not quantitative analysis of the

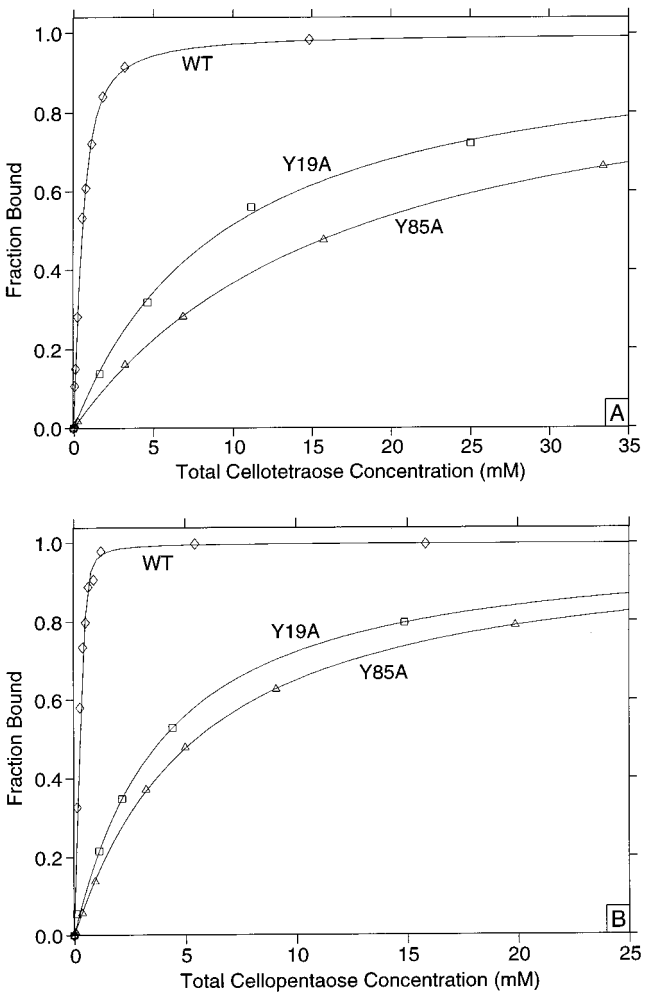

FIGURE 5: Association constants of CBD_{N1} for cellotetraose (A) and cellopentaose (B) were determined from titration curves monitored by $^1H-^{15}N$ spectroscopy. The normalized amide chemical shift of wild-type CBD (◇), Y19A (□), and Y85A (△) is plotted as a function of cellooligosaccharide concentration in each plot. Each solid line represents the titration isotherms obtained by fitting the observed data points to the Langmuir binding model.

effect of a mutation on these CBDs. To the first approximation, the HSQC spectra of the three proteins are very similar, again indicating that the amino acid replacements do not markedly perturb the structural environments of the backbone and side-chain-containing N−H groups. The spectra of the

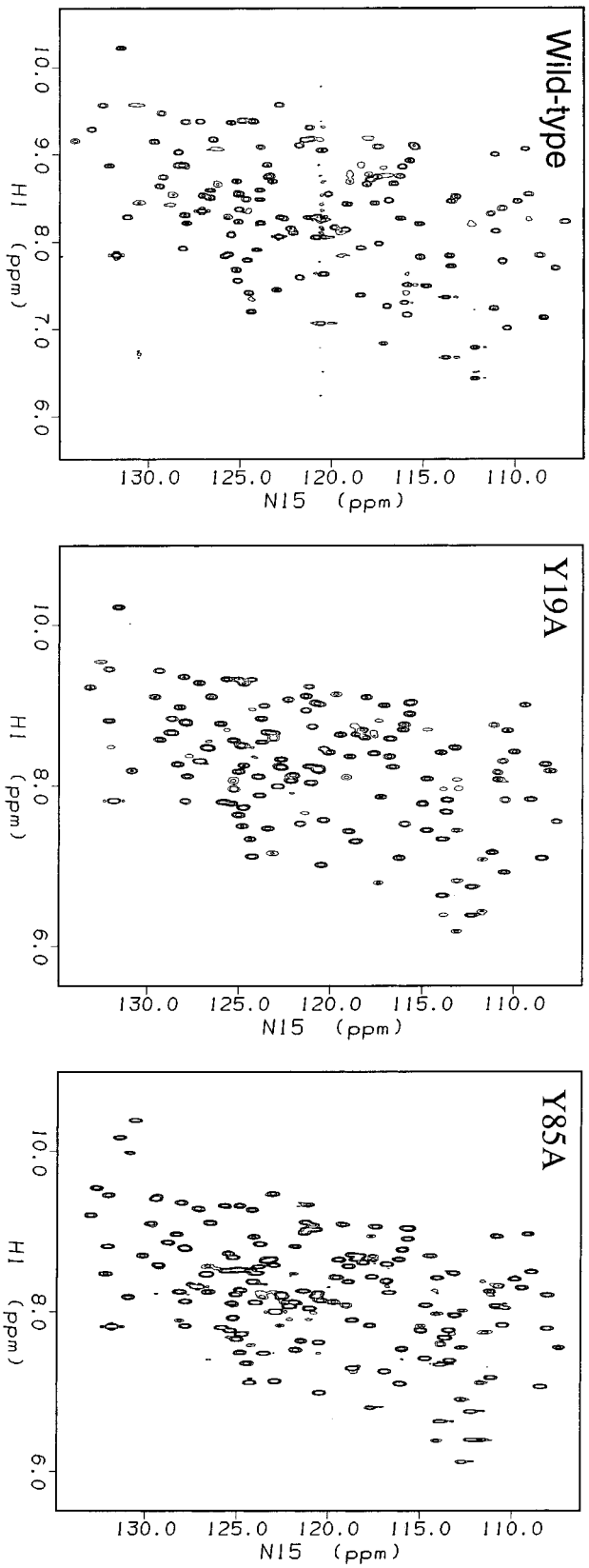

FIGURE 6: $^1H-^{15}N$ heteronuclear single quantum coherence (HSQC) spectra of wild-type CBD_{N1}, Y85A, and Y19A. Each cross-peak that arises from a backbone amide or side-chain asparagine, glutamine, or tryptophan residue is a sensitive marker of possible structural perturbations in the protein arising from the amino acid substitution. The overall similarity of the spectra indicate that the amino acid substitutions do not markedly perturb the structure of CBD_{N1}. Data were acquired on a Varian Unity 500 MHz spectrometer at 30 °C with ^{15}N-labeled samples of protein in 50 mM phosphate buffer, pH 7, supplemented with 10% D_2O.

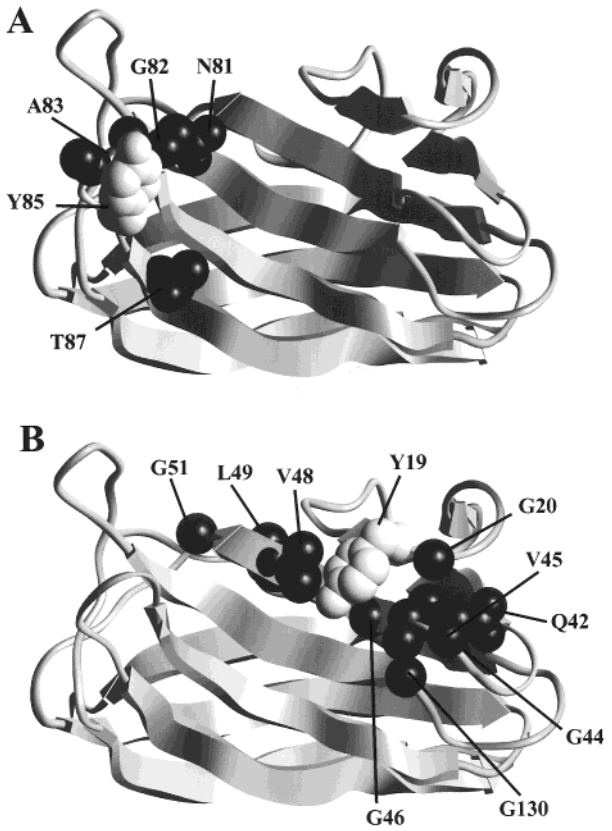

FIGURE 7: Rasmol structures of CBD_{N1} illustrating the chemical shifts perturbed in the heteronuclear single quantum coherence (HSQC) spectra for (A) Y85A and (B) Y19A relative to the wild-type protein. The side chains of Y85 and Y19 are included in dark gray in panels A and B, respectively, for reference purposes.

Y85A and Y19A proteins were not explicitly reassigned, and therefore a detailed comparison was made by assuming that peaks with the same chemical shifts in the spectra of the wild-type and mutant proteins arise from the same N−H groups. By exclusion, those with different shifts in the spectra of the proteins are taken to be perturbed by the mutation and identified on the basis of their previously determined assignments in wild-type CBD_{N1}. Overlapping peaks or peaks from amides whose chemical shifts are influenced by Ca^{2+} binding (*42*) were neglected in this analysis.

The $^1H-^{15}N$ HSQC spectrum of Y85A differs most significantly from that of wild-type CBD_{N1} at the chemical shifts of the amides of residues N81, G82, A83, and T87. These residues are all in close proximity to position 85 (Figure 7A). The chemical shift changes could arise from subtle changes in the backbone of CBD_{N1} near position 85 due to the amino acid replacement or from changes in their magnetic environments due to removal of the aromatic ring of the tyrosine. Regardless, these measurements indicate that the structural perturbations due to the replacement of Y85 by alanine are relatively small and highly localized to the region around this position.

The $^1H-^{15}N$ HSQC spectrum of Y19A differs from CBD_{N1} at nine chemical shifts, corresponding to the amides of residues G20, Q42, G44, V45, G46, V48, L49, G51, and G130. The positions of these residues relative to Y19 are indicated in Figure 7B. In this case, it is doubtful that aromatic ring current effects (caused by removal of the phenol ring of Y19) are responsible for the chemical shift

perturbations of all nine residues. The shielding of residues such as G20, G44, G46, and G48 could be affected by removal of the phenol ring, but L49 and G51 are more distal to the mutation site. Moreover, the perturbed residues belong to a single β-strand or are part of two adjoining loop regions near Y19. We therefore conclude that the substitution of Y19 by alanine perturbs the backbone structure of the protein at positions close to the site. However, as with Y85A, the effects are localized to the site of mutation.

DISCUSSION

General Comments. The NMR-derived structure of CBD_{N1} indicates a putative binding cleft lined with hydrophobic residues and flanked by hydrophilic groups. The ^1H and ^{15}N resonances of many of these residues shift significantly on titration with carbohydrate, suggesting that they interact directly with the ligand. In our model, the cellooligosaccharide molecule lies inside a cleft, with the pyranose rings stacked against hydrophobic residues, and hydrogen bonds formed between the carbohydrate hydroxyl groups and hydrophilic residues of the CBD. In this work, the contribution of 10 hydrophilic residues to the binding of CBD_{N1} was tested by site-directed mutagenesis.

The alanine substitution of CBD_{N1} at 10 positions resulted in similar relative changes in the affinities of the proteins on PASA and barley β-glucan relative to the wild-type protein. PASA is an insoluble allomorph of cellulose that is highly amorphous in composition (*43*). Barley β-glucan differs from PASA in two important ways. First, the polymer is soluble, and second, it is characterized by repeating units of two or three β-1,4 linkages (on average), followed by a β-1,3 linkage. Insoluble cellulose is comprised solely of β-1,4 linkages. Because each mutation studied had a similar effect on CBD binding to each substrate, it would appear that all 10 residues in the binding cleft recognize the same features in PASA and barley β-glucan, despite differences in the macroscopic and chemical properties of each substrate. This suggests that CBD_{N1} interacts with single cellulose chains in PASA, irrespective of the fact that PASA is an insoluble compound, and supports previous studies indicating that five consecutive glucopyranosyl residues comprise the complete binding site of CBD_{N1}, regardless of whether that substrate is soluble or insoluble (*28*, *29*).

Inspection of Table 1 reveals that each mutant had a higher affinity for PASA than for barley β-glucan. This is due, at least in part, to differences in binding temperature. All adsorption isotherms were performed at 4 °C, while affinity electrophoresis experiments were conducted at room temperature, and are subject to additional temperature effects from the heating of the gels. Both DSC and ITC results have demonstrated that the binding affinity of CBD_{N1} decreases with increasing temperature (*29*, *31*). In addition, ITC studies illustrated that the binding affinity of wild-type CBD_{N1} for barley β-glucan and cellopentaose is similar at 30 °C (*29*).

The average binding saturation value (N_o) for wild-type CBD_{N1} was 6.85 μmol/g of PASA. Compared to the relative changes in affinity, binding saturation values (N_o) did not change appreciably for most mutants, varying between 4.0 and 7.0 μmol/g cellulose. Interestingly, the lowest measured N_o values were for those mutants with the weakest overall affinities. This may reflect the problems of extrapolation discussed earlier. However, another explanation is that insoluble cellulose is a heterogeneous substrate containing an array of both high- and low-affinity binding sites (*32*). Reductions in affinity may exclude CBD binding to the low energy sites, thus reducing the total N_o value.

Individual Mutations. The 10 residues studied by site directed mutation can be organized into three separate classes on the basis of their relative contribution to binding. In one class, exemplified by residues D90, Q80, and T87, mutation to alanine decreases the binding affinity by less than 2-fold. On the basis of their weak contributions to binding, it is unlikely that D90, Q80, or T87 interacts directly with substrate. However, their removal does result in a modest decrease in binding affinity, suggesting that, in the absence of direct interactions with ligand, these residues must have a supporting role in maintaining the geometry of the binding site, perhaps by holding the principal binding site residues in proper position. The solved structure of CBD_{N1} (*20*) provides further insights into the role of Q80, whose side chain is located in a loop between β-strands and extends away from the binding cleft of CBD_{N1}. Such positioning would make it nearly impossible for that side chain to interact with substrate, suggesting that Q80 does play an indirect role, albeit small, in helping maintain the active conformation of the protein.

The second class of residues shows more significant reductions to the binding affinity of CBD_{N1} upon mutation to alanine and includes residues R75, N81, Q124, Q128, and N50. On the basis of their contribution to binding, it is probable that these residues interact directly with ligand through either hydrogen bonds or van der Waals interactions, though some structure-stabilizing role is also possible.

The final group of residues mutated in this study includes Y19 and Y85. These, upon mutation to alanine, cause a reduction in CBD binding affinity that is greater than 50-fold on PASA, barley β-glucan, cellotetraose, and cellopentaose. Such large contributions to binding, combined with the structural data presented, suggest a combination of hydrogen-bonding and van der Waals interactions at the interface between either tyrosine and substrate. Inspection of the structure of CBD_{N1} reveals that although the binding cleft spans five glucopyranosyl units, the two tyrosine side chains are separated by approximately the end-to-end distance of cellotetraose. Consistent with this observation, the removal of either tyrosine reduces binding to both cellotetraose and cellopentaose. Furthermore, studies with a nitroxide spin-labeled derivative of cellotetraose reveal that the sugar can bind in multiple orientations across the cleft of CBD_{N1} (*30*). Thus, the effects of the tyrosine substitutions are likely an average of the effects of binding with the reducing end of the sugar nearest one or the other edge of the β-sheet face of the protein.

Thermodynamic Implications. The calculated $\Delta\Delta G$ values [$\Delta\Delta G = -RT \ln (K_{a,mutant}/K_{a,wt})$] for most of the mutants (Table 1) are well within the energetic range for the enthalpy of a hydrogen bond (*42*). Unfortunately, the $\Delta\Delta G$ values do not indicate that these residues form hydrogen bonds with ligand since the relationship between $\Delta\Delta G$ and $\Delta\Delta H$ is often very difficult to predict. In general, $\Delta\Delta G$ values are never as large as $\Delta\Delta H$ values because of enthalpy/entropy compensation ($\Delta G = \Delta H - T\Delta S$) (*43*). Increased enthalpic

contribution is always associated with an entropic cost in terms of the increased order imposed on the molecules involved. Understanding the enthalpy of binding and its correlation to $\Delta\Delta G$ is also difficult due to the complexity of binding. Binding is never as simple as bond formation in solution. Protein−ligand formation is usually the result of multiple displacement reactions where water molecules, originally hydrogen-bonded to ligand receptor groups or the ligand itself, are subsequently displaced upon formation of the protein−ligand complex (*44*). Similarly, intramolecular interactions between chemical groups within the protein or ligand may also be displaced during complexation, and global conformational changes in the protein may occur. In mutagenic studies, the situation is even more complex since mutation can cause fine structural changes in the protein (*23*, *45*−*48*). These spatial changes may, in combination with the chemical changes induced by mutation, influence the enthalpy and entropy of binding considerably. Predicting this effect in terms of $\Delta\Delta G$ is usually impossible. For instance, the mutation to alanine or phenylalanine of several streptavidin residues involved in hydrogen bonds to biotin all resulted in an increased ΔG (i.e., decreased affinity), though both increases and decreases in ΔH were noted in the mutants (*49*).

Paradigm of Carbohydrate Binding Proteins. Carbohydrates display both polar and apolar characteristics. While the periphery of each sugar monomer clearly displays a high degree of polarity, the glucose ring is quite hydrophobic. Consequently, one would expect proteins to use hydrogen bonds and polar and nonpolar van der Waals contacts to maximize their interaction with each saccharide unit of a carbohydrate structure. Hydrogen bonds, because of their strength and directional nature, are thought to be responsible for binding specificity, while van der Waals interactions stabilize the binding complex. These types of contacts are augmented by aromatic residues, chiefly tyrosine and tryptophan. They can generate significant van der Waals forces through base stacking with glucopyranosyl rings and also have the ability to serve as hydrogen-bond donors or acceptors with peripheral glucose hydroxyl groups. So, it is not surprising that tyrosine mediates the binding of CBD_{N1} to cellulosic substrates; nor is it surprising that tyrosines are commonly found as important binding site residues in several protein−carbohydrate interactions (*23*, *46*, *50*−*54*).

CBD_{N1} can be discussed in terms of two classification systems. First, CBD_{N1} can be assigned to the more general system of Quiocho et al. (*55*) for classifying carbohydrate binding proteins. Or second, CBD_{N1} can be compared to other cellulose binding proteins the CBD classification system of Tomme et al. (*6*, *7*).

CBD_{N1} can be grouped into the system of Quiocho et al. (*55*) as a group II carbohydrate binding protein. The CBD has a surface-exposed binding site, and the magnitude of its demonstrated affinity for substrate is very similar to those of other group II proteins, which include immunoglobulins, lectins, the phosphorylase storage site and starch binding domains. In contrast, group I carbohydrate binding proteins contain an enclosed binding site and illustrate binding affinities typically in the range of 10^6 M^{-1}. Examples of group I proteins include periplasmic sugar transport proteins, the phosphorylase active site, and the *lacI* family of repressors (*55*, *56*).

In the system of Tomme et al. (*6*, *7*), CBD_{N1} is classified as a family IV CBD. It is the first family IV CBD to be solved structurally (*20*), and have its binding site characterized by mutagenesis. Moreover, CBD_{N1} is only the fourth CBD, along with the family I protein CBD_{CBHI} (*22*, *23*) and the family II proteins, CBD_{CenA} (*25*) and CBD_{XylA} (*24*, *27*), to be characterized by site-directed mutagenesis.

ACKNOWLEDGMENT

We thank Al Boraston and Brad McLean for their input in the quantitative analysis of binding and Emily Kwan for preparing PASA. We also thank NSERC and PENCE for supplying the necessary funding to complete this research.

REFERENCES

1. Henrissat, B., Cleiyssens, M., Tomme, P., Lemesle, L., and Mornon, J. P. (1989) *Gene 81*, 83−95.
2. Gilkes, N. R., Henrissat, B., Kilburn, D. G., Miller, R. C., Jr., and Warren, R. A. J. (1991) *Microbiol. Rev. 55* (2), 303−315.
3. Henrissat, B., and Bairoch, A. (1993) *Biochem. J. 293*, 781−788.
4. Henrissat, B., Teeri, T. T., and Warren, R. A. J. (1998) *FEBS Lett. 425*, 352−354.
5. Coutinho, J. B., Gilkes, N. R., Warren, R. A. J., Kilburn, D. G., and Miller, R. C., Jr. (1992) *Mol. Microbiol. 6* (9), 1243−1252.
6. Tomme, P., Warren, R. A. J., Miller, R. C. Jr., Kilburn, D. G., and Gilkes, N. R. (1995) in *Enzymatic Degradation of Insoluble Polysaccharides* (Saddler, J. M., and Penner, M., Eds.) pp 142−161, American Chemical Society, Washington, DC.
7. Tomme, P., Boraston, A., Creagh, A. L., Gilkes, N. R., Haynes, C. A., Kormos, J., McLean, B., Sturch, K., Warren, R. A. J., and Kilburn, D. G. (1998) *J. Chromatogr. B: Biomed. Sci. Appl. 715* (1), 283−296.
8. Van Tilbeurgh, H., Tomme, P., Claeyssens, M., Bhikhabhai, R., and Pettersson, G. (1986) *FEBS Lett. 204*, 223−227.
9. Tomme, P., Van Tilbeurgh, H., Pettersson, G., Van Damme, J., Vandekerckhove, J., Knowles, J., Teeri, T., and Claeyssens, M. (1988) *Eur. J. Biochem. 170*, 575−581.
10. Coutinho, J. B., Gilkes, N. R., Kilburn, D. G., Warren, R. A. J., and Miller, R. C., Jr. (1993) *FEMS Microbiol. Lett. 113*, 211−218.
11. Reinikainen, T., Teleman, O., and Teeri, T. T. (1995) *Proteins: Struct. Funct., Genet. 22*, 392−403.
12. Hall, J., Black, G. W., Ferriera, L. M. A., Millward-Saddler, S. J., Ali, B. R. S., Hazlewood, G. P., and Gilbert, H. J. (1995) *Biochem. J. 309*, 749−756.
13. Garda, A. L., Fernández-Abalos, J. M., Sánchez, P., Ruiz-Arribas, A., and Santamaria, R. I. (1997) *Biochem. J. 324*, 403−411.
14. Din, N., Gilkes, N. R., Tekant, B., Miller, R. C. Jr., Warren, R. A. J., and Kilburn, D. G. (1991) *Bio Technology 9*, 1096−1099.
15. Ong, E., Gilkes, N. R., Miller, R. C., Jr., Warren, R. A. J., and Kilburn, D. G. (1993) *Biotechnol. Bioeng. 42*, 401−409.
16. Tormo, J., Lamed, R., Chirino, A. J., Morag, E., Bayer, E. A., Shoham, Y., and Steitz, T. A. (1996) *EMBO J. 15*, 5739−5751.
17. Sakon, J., Irwin, D., Wilson, D. B., and Karplus, P. A. (1997) *Nat. Struct. Biol. 4* (10), 810−817.
18. Kraulis, P. J., Clore, G. M., Nilges, M., Jones, T. A., Pettersson, G., Knowles, J., and Gronenborn, A. (1989) *Biochemistry 28*, 7241−7257.
19. Xu, G. Y., Ong, E., Gilkes, N. R., Kilburn, D. G., Muhandiram, D. R., Harris-Brandts, M., Carver, J., Kay, L., and Harvey, T. (1995) *Biochemistry 34*, 6993−7009.
20. Johnson, P. E., Joshi, M. D., Tomme, P., Kilburn, D. G., and McIntosh, L. P. (1996) *Biochemistry 35*, 14381−14394.

21. Brun, E., Moriaud, F., Gans, P., Blackledge, M. J., Barras, F., and Marion, D. (1997) *Biochemistry 36*, 16074−16086.
22. Reinkainen, T., Ruohonen, L., Nevanen, T., Laaksonen, L., Kraulis, P., Jones, T. A., Knowles, J. K. C. and Teeri, T. T. (1992) *Proteins: Struct., Funct., Genet. 14*, 475−482.
23. Linder, M., Mattinen, M.-L., Kontteli, M., Lindeberg, G., Ståhlberg, J., Drakenberg, T., Reinkainen, T., Pettersson, G., and Annila, A. (1995) *Protein Sci. 4*, 1056−1064.
24. Poole, D. M., Hazelwood, G. P., Huskisson, N., Virden, R., and Gilbert, H. J. (1993) *FEMS Microbiol. Lett. 106*, 77−84.
25. Din, N., Forsythe, I. J., Burtnick, L. D., Gilkes, N. R., Miller, R. C., Jr., Warren, R. A. J., and Kilburn, D. G. (1994) *Mol. Microbiol. 11* (4), 747−755.
26. Bray, M. R., Johnson, P. E., Gilkes, N. R., McIntosh, L. P., Kilburn, D. G., and Warren, R. A. J. (1996) *Protein Sci. 5*, 2311−2318.
27. Nagy, T., Simpson, P., Williamson, M. P., Hazlewood, G. P., Gilbert, H. J., and Orosz, L. (1998) *FEBS Lett. 429*, 312−316.
28. Johnson, P. E., Tomme, P., Joshi, M. D., and McIntosh, L. P. (1996b) *Biochemistry 35*, 13895−13906.
29. Tomme, P., Creagh, L. A., Kilburn, D. G., and Haynes, C. A. (1996) *Biochemistry 35*, 13885−13894.
30. Johnson, P. E., Brun, E., MacKenzie, L., Withers, S. G., and McIntosh, L. P. (1999) *J. Mol. Biol. 287*, 609−625.
31. Creagh, A. L., Koska, J., Johnson, P. E., Tomme, P., Joshi, M. D., McIntosh, L. P., Kilburn, D. G., and Haynes, C. A. (1998) *Biochemistry 10*, 3529−3537.
32. Creagh, A. L., Ong, I., Jervis, E., Kilburn, D. G., and Haynes, C. A. (1996) *Proc. Natl. Acad. Sci. U.S.A. 93*, 12229−12234.
33. Wood, T. M. (1988) in *Methods in Enzymology, Vol. 160, Biomass, Part A, Cellulose and Hemicellulose* (Wood, W. A., and Kellog, S. T., Eds.) pp 19−26, Academic Press, Toronto, Ontario, Canada.
34. Graham, R. W., Greenwood, J. M., Warren, R. A. J., Kilburn, D. G., and Trimbur, D. E. (1995) *Gene 158*, 51−54.
35. Yanisch-Perron, C., Vieira, J., and Messing, J. (1988) *Gene 33*, 103−119.
36. Hanahan, D. (1983) *J. Mol. Biol. 166*, 557−580.
37. Nossal, N. G., and Heppel, L. A. (1966) *J. Biol. Chem. 24*, 3055−3062.
38. Takeo, K., and Nakamura, S. (1972) *Arch. Biochem. Biophys. 10*, 1−7.
39. Takeo, K., Kuwahara, A., Nakayama, H., and Nakamura, S. (1975) *Protides Biol. Fluids 23*, 645.
40. Takeo, K., and Kabat, E. A. (1978) *J. Immunol. 121* (6), 2305−2311.
41. Kormos, J. (1999) M.Sc. Thesis, Department of Microbiology and Immunology. University of British Columbia, Vancouver, British Columbia, Canada.
42. Johnson, P. E., Creagh, A. L., Brun, E., Joe, K., Tomme, P., Haynes, C. A., and McIntosh, L. P. (1998) *Biochemistry 37*, 12772−12781.
43. Lee, S. B., and Kim, I. H. (1983) *Biotechnol. Bioeng. 25*, 33−51.
44. Fersht, A. R., Shi, J. P., Knill-Jones, J., Lowe, D. M., Wilkinson, A. J., Blow, D. M., Brick, P., Carter, P., Waye, M. M. Y., and Winter, G. (1985) *Nature 314*, 235−238.
45. Dunitz, J. D. (1995) *Chem. Biol. 2* (11), 709−712.
46. Connelly, P. R., Aldape, R. A., Bruzzese, F. J., Chambers, S. P., Fitzgibbon, M. J., Fleming, M. A., Itoh, S., Livingston, D. J., Navia, M. A., Thomson, J. A., and Wilson, K. P. (1994) *Proc. Natl. Acad. Sci. U.S.A. 91*, 1964−1968.
47. Kline, T. P., and Mueller, L. (1992) *Int. J. Pept. Protein Res. 39*, 111−116.
48. Naghora, H., Harata, K., Muraki, M., and Jigami, Y. (1995) *Eur. J. Biochem. 233*, 27−34.
49. Castro, M. J. M., and Anderson, S. (1996) *Biochemistry 35*, 11435−11446.
50. Siebert, H. C., Adar, R., Arango, R., Burchert, M., Kaltner, H., Kayser, G., Tajkhorshid, E., von der Lieth, C. W., Kaptein, R., Sharon, N., Vliegenthart, J. F., and Gabius, H. J. (1997) *Eur. J. Biochem. 249* (1), 27−38.
51. Klumb, L. A., Chu, V., and Stayton, P. S. (1998) *Biochemistry 37*, 7657−7663.
52. Penninga, D., van der Vee, B. A., Knegtel, R. M., van Hijum, S. A., Rozeboom, H. J., Kalk, K. H., Dijkstra, B. W., and Dijkhuizen, L. (1996) *J. Biol. Chem. 271*, 32777−32784.
53. Zhu, K., Bressan, R. A., Hasegawa, P. M., and Murdock, L. L. (1996) *FEBS Lett. 390* (3), 271−274.
54. Burrows, L., Iobst, S. T., and Drickamer, K. (1997) *Biochem. J. 324*, 673−680.
55. Moreno, E., Teneberg, S., Adar, R., Sharon, N., Karlsson, K. A., Angstrom, J. (1997) *Biochemistry 36* (15), 4429−4437.
56. Mullin, N. P., Hitchen, P. G., and Taylor, M. E. (1997) *J. Biol. Chem. 272* (9), 5668−5681.
57. Quiocho, F. A., Spurlino, J. C., and Rodseth, L. E. (1997) *Structure 5* (6), 997−1015.
58. Quiocho, F. A. (1993) *Biochem. Soc. Trans. 21*, 442−448.
59. Brun, E. Johnson, P. E., Creagh, A. L., Tomme, P., Webster, P., Haynes, C. A., and McIntosh, L. P. (2000) *Biochemistry 39*, 2445−2458.

BI000607S